This is the accepted manuscript version of the paper: T. Fapanni, M. Serpelloni and E. Sardini, "Uncertainty Sources in Aerosol Jet Printed and Flexible Electrochemical Sensors," *2022 IEEE International Workshop on Metrology for Industry 4.0 & IoT (MetroInd4.0&IoT)*, Trento, Italy, 2022, pp. 245-249, doi: 10.1109/MetroInd4.0IoT54413.2022.9831522.
The final published version and copyright permissions are available on https://ieeexplore.ieee.org/document/9831522

Uncertainty Sources in Aerosol Jet Printed and Flexible Electrochemical Sensors

Tiziano Fapanni
Department of Information Engineering
University of Brescia
Brescia, Italy
t.fapanni@unibs.it

Mauro Serpelloni
Department of Information Engineering
University of Brescia
Brescia, Italy
mauro.serpelloni@unibs.it

Emilio Sardini
Department of Information Engineering
University of Brescia
Brescia, Italy
emilio.sardini@unibs.it

***Abstract*— Electrochemical sensors are nowadays used in a wide set of applications even though they still present major issues that weaken their metrological characteristics. Among those, noise is interesting because determines the lowest detectable concentration and allows developing better models for electrochemical sensors. In this work, a set of flexible electrochemical sensors produced by Aerosol Jet Printing (AJP) are analyzed to identify their different noise and uncertainty sources. Different conditions such as analyte concentration variations and temperature fluctuations are taken into consideration. Effects on noise of processes inherently connected with the transduction principle such as double-layer capacitance and mass transport were observed as well as a correlation between the analyte concentration and the overall noise. Thermal effects analysis revealed an overall increment of the noise level up to 52.4% in a 10 °C interval while a variation of over 100% of the mean output current on the same interval are recorded. According to the results presented in this work, noise and temperature effects should be taken into consideration in the design of novel electrochemical devices to improve their reliability in uncontrolled conditions.**

Keywords*— *electrochemical sensors, noise, SNR chronoamperometry

I. Introduction

Electrochemical sensors are attracting great interest in the scientific community thanks to their ease of use and reduced cost that allow their employment in a wide set of applications such as food safety, environmental pollution control, and the detection of biomolecules and proteins [1]–[7]. In this frame where electrochemical sensors acquired great relevance, printed electronics was explored to fabricate those devices because it offers great opportunities such as miniaturization and customization as well as integration of devices on non-conventional substrates that could be both 3D and/or flexible. Moreover, flexibility is a key paradigm that can improve user comfort in a spectrum of biomedical and wearable devices both for point of care diagnostics and mobile health [8]. This last advantage requires the use of non-contact printing techniques such as aerosol jet printing (AJP). This technology was chosen for this application thanks to its peculiar characteristics as the possibility to use ink with a wide spectrum of viscosities and quick prototyping ([9], [10]). Its peculiar non-contact production process uses gases to depose the functional inks. Three gas flows control the AJP process. The first one (atomizer flow) atomizes the functional ink and carries the produced aerosol [11]. Then exhaust flow controls the aerosol particle dimension and lastly, the sheath flow focuses the aerosol on the nozzle. The three flows can be optimized to obtain lines with width from 10 µm up to 3 mm and thickness ranging from hundreds of nanometers up to a few micrometers. AJP is reported in the literature as a viable technology to produce electrochemical sensors [7], [9], [10], [12]. Even though they present many advantages, those kinds of sensors are affected by many metrological issues, mostly regarding sensitivity, selectivity, repeatability, limit of detection (LOD) and signal to noise ratio (SNR) [2], [5]. Many efforts are devoted in the scientific community to address these issues. Among the solutions proposed in the literature, both organic and inorganic functionalization are explored and seem to be providing relevant improvements. Lately, inorganic materials are being of great interest thanks to the advantages provided by nanomaterials that are promising to increase the surface area and for their enzyme mimetic effect [13], [14]. Among the nanomaterials, carbon-based ones have been widely explored thanks to their advantages such as their conductivity, flexibility, potential mass production, chemical and thermal stability[15]. These techniques are often used to address sensitivity and selectivity issues, but to further improve the quality of the measurements uncertainty control is fundamental. Uncertainty is related to the used instrumentation as well as the intrinsic noise produced by the sensor. The latter is important to allow the detection of low concentrations of analytes, design improved next-generation devices and develop better models for electrochemical sensors [16]. Excluding electromagnetic narrowband interferences, one of the main components that contributes to uncertainty in electronic systems and sensors is due to thermal effects. Moreover, temperature effects are shown to influence the overall behavior of electrochemical sensors [17]. In this work, the signal produced by AJP-printed electrochemical sensors during chronoamperometry (CA) is analyzed to identify their different noise and uncertainty sources.

II. Materials and Methods

A. Sensors production process

Starting from previous work [9], [10], we designed simple three-electrode cells composed of working (WE), reference (RE) and counter (CE) electrodes. We propose a three-layer device produced using silver-silver chloride ink chloride (AgCl ink, XA-3773, Fujikura Kasei Co. Ltd., Shibakouen Minato-ku, Tokyo, Japan) for interconnections, pads and the reference electrode (RE); A carbon layer (C ink, EXP 2652-28, Creative Materials Inc., Ayer, MA, USA) was deposed on top of the working and counter electrodes (WE and CE

respectively) to provide a stable electrochemical substrate as well as a suitable substrate for the further functionalization performed with carbon nanotubes (Multi-Walled Carbon Nanotubes ink, Nink 1000, NANOLAB, Waltham, MA, USA). A Kapton substrate was selected as flexible substrate due to its excellent flexibility, thermal stability and chemical durability. The production process was performed optimized to try to reduce inter-sensor variability. The devices were printed in two rows parallelizing the production of the devices. An Aerosol Jet Printer (AJ300, Optomec, Albuquerque, NM, USA) with a 750 µm head was employed to fabricate the bare devices. The Kapton substrate for each lot is at first cleaned in ethanol to remove possible contaminants and increase the adhesion between ink and substrate. Then AgCl ink is deposed and cured at 125 °C for 30 minutes. Next, WE and CE are coated with carbon ink and then cured at 175 °C for 15 minutes. Then, the electrodes were AJP-functionalized using a 300 µm head and CNT ink. The nanostructured ink was thermally cured for 20 minutes before testing. The produced electrodes are shown in figure 1.

B. Preliminary Evaluations

Different tests were carried on analyzing the electrochemical behavior of the devices. All the tests were performed using a portable potentiostat Palmsens3 EIS (Palmsens, Compact Electrochemical Interfaces, Houten, Utrecht, The Netherlands). Those tests defined a stable potential window of [-0.15; 1]V in Phosphate Buffered Saline (PBS). Then, different chronoamperometry (CVs) were performed in ferro/ferricyanide ($[Fe(CN)_6]^{3-/4-}$) in PBS solutions at different concentrations (2 mM, 4 mM, 6 mM and 8 mM) at a fixed scan rate ($\nu = 0.2\,V/s$). The shape of the voltammograms was evaluated and the peak position and amplitude were compared.

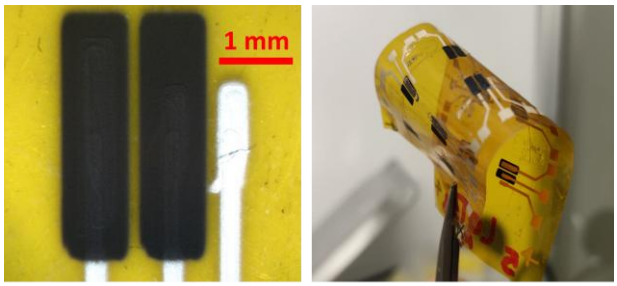

Fig. 1. Sensors produced with a focus on their active area (a) and their flexibility (b)

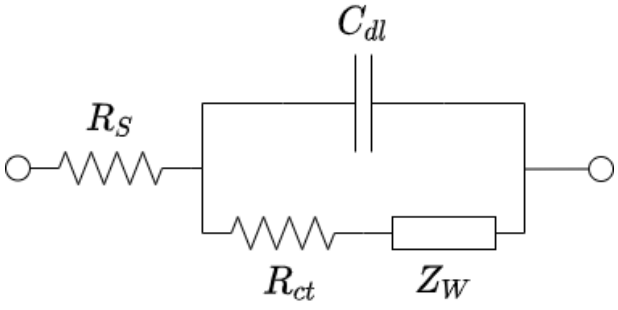

Fig. 2. Randles circuit model for an electrode/electrolyte interface.

C. Electrochemical Cell Impedance

The electrochemical cell impedance was also evaluated to obtain information on the equivalent model of the cell. In the literature, many are the proposed models, but often the most used is the Randles circuit shown in figure 2. C_{dl} represents the double-layer capacitance and R_s is the bulk solution resistance. R_{ct} (charge transfer resistance) and Z_W (Warburg impedance) represent the whole charge transfer process. [18] Those models are often referred as useful to understand the noise components of the sensors [19]. In order to obtain its impedance, the cell was polarized at 1V and 0.1V sinusoidal small signals at different frequencies were superimposed to obtain the impedance spectrum of the cell. The measurements were performed from 10 mHz to 50 kHz. The experiments were carried on changing two different parameters: at first the analyte concentration and then the stirring frequency. We chose ferro/ferricyanide as analyte and we changed different concentrations (0 mM, 1 mM, 2 mM and 3 mM).

D. Measurement Setup for Noise Collection

To extract the noise levels, the electrodes were immersed in 20 mL of Phosphate Buffered Saline (PBS) solution that is stirred at different frequencies through an ARGO LAB M2-D Pro magnetic stirrer (Giorgio Bormac S.r.l., Carpi, Italy). Noise levels were evaluated at different hydrogen peroxide concentrations ranging from 100 µM to 500 µM through a single chronoamperometry (CA) where each 200s the concentration is stepped. The applied potential was set above the oxidation peak for the analyte at 1V. During this experiment the stirrer was set to 490 rpm. The experiment was carried on with the abovementioned Palmsens3 EIS at a sampling frequency of 5 Hz. The collected signals were elaborated through MATLAB 2019b. In particular, the output signal is expected to be a constant current. From this consideration, the average current is subtracted from the measured signal and the resulting one is considered as the output referred noise of our experiment. This is composed by both the noise introduced by the sensor and by the noise introduced by the interconnections, the electronic frontend and the digitalization. All the noise components that are related with the measurement setup were evaluated replacing the sensor with a 220 kΩ resistor. A resistor produces a white noise with a power spectral density (PSD) as reported in equation 1, where k represents the Boltzmann constant and T the absolute temperature.

$$S_{ni} = \frac{4kT}{R} \quad (1)$$

The noise recorded in this condition produced a PSD constant over our frequencies of interest, with a mean power of approximately $2 \cdot 10^{-21} \frac{A^2}{Hz}$ and can be used as a background noise level.

E. Temperature Influence

A test was carried on assessing the thermal noise contribution on the signal. A sensor was immersed in 20 mL stirred PBS solution and a CA was recorded. After 300s at 20 °C, the solution was heated up to 48 °C using the abovementioned stirrer. The solution temperature was monitored during the

whole process. The recorded signal's noise was evaluated in the two situations. In a similar setup, a second electrode underwent a CA while the stirrer temperature was stepped from 25 °C to 50 °C to evaluate how the temperature influences the output current of the printed electrochemical sensors. To monitor the temperature a commercial PT100 sensor was immersed in the solution. A custom virtual instrument on LabVIEW was designed to sample each second the resistance of the sensor through a Hewlett–Packard 34401a (HP, Palo Alto, CA, USA) using a 4-wire technique.

III. Results and Discussion

A. Preliminary Evaluation

The preliminary evaluations produce a set of well-defined voltammograms. An example can be seen in figure 3. The sensors presented a fully reversible behavior with a peak separation around 150 mV. The relationship between the peak current and the applied ferro/ferricyanide concentration presented an optimal linearity (R^2>0.999) showing a sensitivity of 12.94 µA/mM.

B. Electrochemical Cell Impedance

The evaluation of the sensor impedance provided different results. Great differences were observed in the impedance between measures in pure PBS and with ferro/ferricyanide (figure 4.a). The main differences are due to the presence of faradic processes when the analyte is in the solution. Those processes mostly influence the charge transfer resistance and the Warburg impedance. Further measures were extracted at different ferro/ferricyanide concentrations (figure 4.b). From these we could estimate a solution resistance of $R_S \approx 37\ \Omega$ and observe similar corner frequencies.

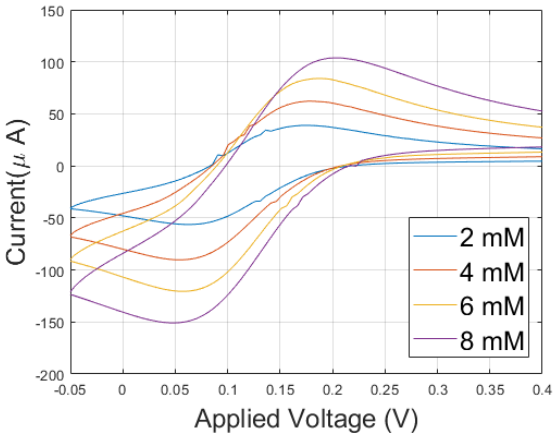

Fig. 3. Voltammograms of the produced sensors performed with 0.2 V/s scan rate in a ferro/ferricyanide in PBS solution at concentration ranging from 2 mM (blue) to 8 mM (purple).

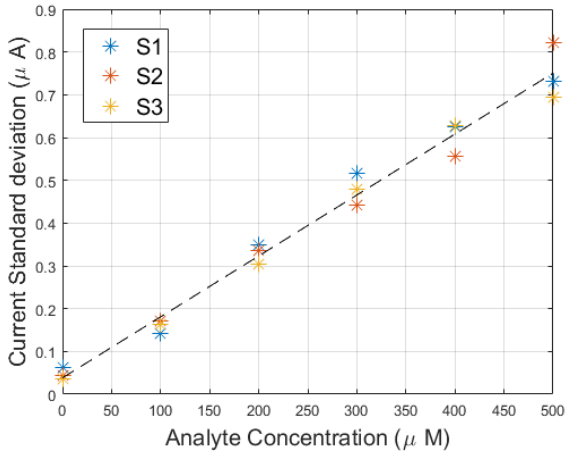

Fig. 5. Standard deviation of the current output recorded at analyte concentrations ranging from 0 µM to 500 µM. Each color represents a sensor, while the dashed black line is the average best fitting line.

C. Noise Analysis

Different levels of noise were recorded at a sampling frequency of 5 Hz on the signal at different concentrations of the analyte. We evaluated the standard deviation of the output current for each concentration step and a linear correlation ($R^2 > 0.997$) between those and the analyte concentration was obtained (figure 5). Moreover, accurate spectral analysis on the noise produced by the sensors was carried on and its power spectral density (PSD) is shown in figure 6. Relevant differences with the previously obtained background noise are observed. The PSD is not constant in frequency, but presents a corner around 0.9 Hz, while the plateau at low frequency is several orders of magnitude higher than background noise. According to [18], this peculiar shape can be seen a superposition of effects related to the transduction principle of the sensors. At high frequencies, for example, mass transport effects are relevant. The current generation relies on the oxidation of species near the electrode surface and the reactants for those reactions are dispersed in the bulk

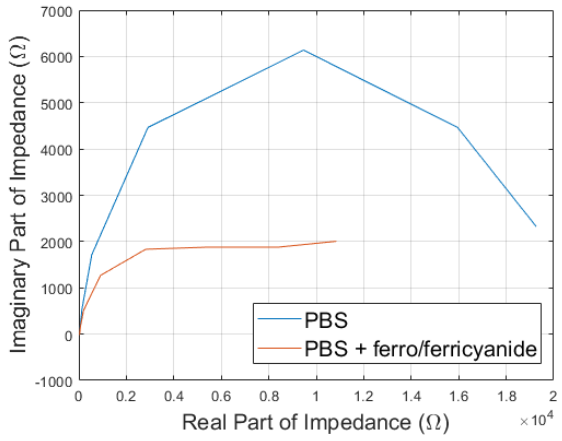

(a)

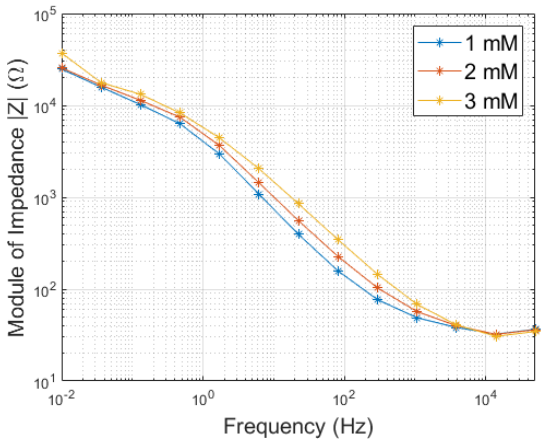

(b)

Fig. 4 Impedance of the electrodes. In (a) the real and imaginary part of the impedance are shown comparing the results obtained in PBS and with 1 mM ferro/ferricyanide. In (b) the impedance module at different ferro/ferricyanide concentration

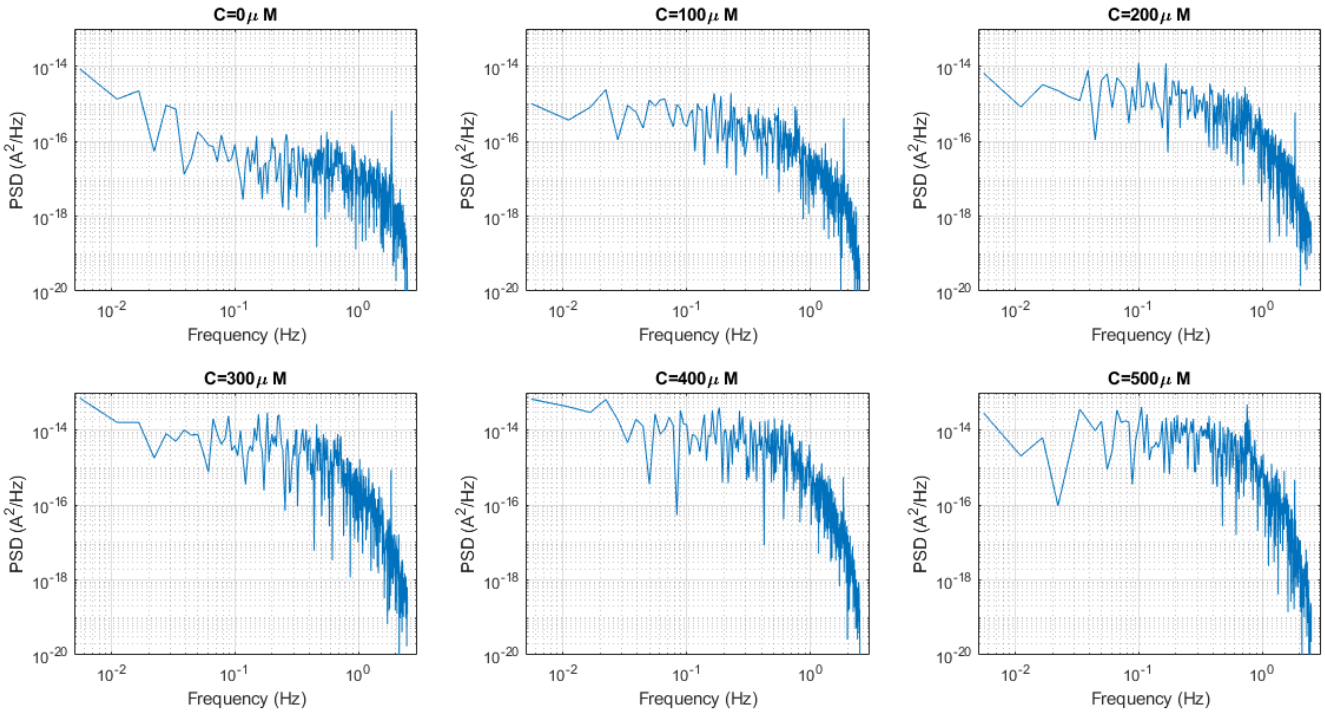

Fig. 6. Power spectral density of the noise collected on chronoamperometry (CA) experiment at analyte concentrations ranging from 0 µM to 500 µM.

solution and are moved to the electrode surface mainly by diffusion. This process requires time and thus shapes the Power Spectral Density (PSD) of the noise resembling a flicker noise. This section of the spectrum is empirically analyzed in [16] where equation 2 is fitted under different operating conditions.

$$N_{flicker} = S(f) = A\, I^2_{avg} / f^{\alpha} \qquad (2)$$

Our measurements agree with the one reported in [16], showing how the α parameters tends to increase with the analyte concentration. On the other hand, at low frequency thermal and shot noise dominate. The former is related to energy dissipation both inside the electrolyte solution and on the electrode-electrolyte interface, while the latter is due to the presence of a potential barrier at the interface. Both those effects produce a white noise with a power that is directly proportional to the average current flowing on the electrochemical cell.

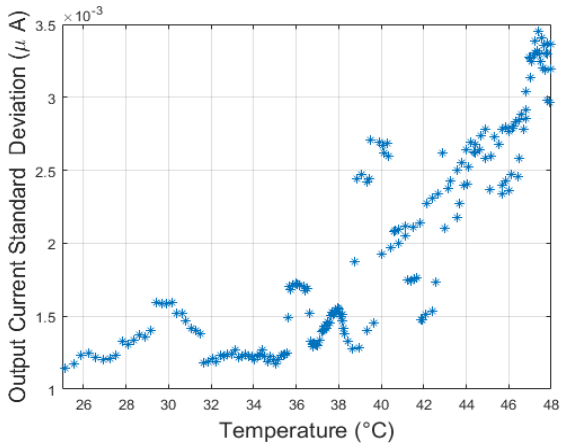

Fig. 7. Standard deviation of the output current signal calculated for different temperatures.

D. Temperature Influence

As exposed before, temperature is one of the main variables that influences the noise and thus the uncertainty in the produced sensors. At first, the noise component was evaluated. Our measurements show (figure 7) how changing the solution temperature leads to an increasing level of noise on the signal. For instance, from 25 °C to 40 °C the noise level increases by 79%. During this experiment, a consistent variation of the average output current of the sensor was observed. This can be a main issue to address to provide reliable measures with these sensors. In order to characterize the process, a new experiment was performed and the output current was recorded while changing the solution temperature between 20 °C and 48 °C. The output current of the sensor was then related to solution temperature as shown in figure 8. This behavior can be explained from the Cottrell equation 3 which express the output current (i_o) as a function of the analyte concentration (C^*) and the surface area of the electrode (A).

$$i_o = \frac{nFAC^*\sqrt{D}}{\sqrt{\pi t}} \quad (3)$$

The diffusion coefficient D is temperature-dependent and can be expressed as Arrhenius exponential function [20] as in equation 4.

$$D = D_0 \exp\left(-\frac{E_D}{RT}\right) \quad (4)$$

From equations 2 and 3, the simplified model presented in equation 5 was extracted.

$$i_o = \sqrt{a \cdot \exp\left(-\frac{b}{T}\right)} \quad (5)$$

This was validated using the experimental data obtaining a coefficient of determination $R^2 > 0.995$.

IV. Conclusions

In this work a set of printed nanostructured electrochemical sensors were considered in order to understand the uncertainty components and influence variables. At first the impedance of the sensor was evaluated and compared to the Randles circuit. Both the effects of the analyte and the electrolyte solution were explored showing a solution resistance of about $37\,\Omega$. First assays show that electrochemical noise is directly proportional with analyte concentrations. The main components that shape the PSD of the sensor noise are explored and those are related to the electrochemical processes underlying the transduction principle of the device. At high frequency, the noise spectrum is limited by mass transport processes that introduce a flicker-like behavior, while at low frequency shot and thermal noise are mostly relevant. The effects of the temperature are then better investigated and they are shown to be dominant not only as a noise source but also as main influence parameters that can change the average output current of the sensor. This behavior was explained using the standard electrochemical theory from which a simplified fitting model was extracted and validated obtaining a coefficient of determination over 0.995. This last result can be used to compensate for the effects of temperature leading to an improvement of the reliability of the sensors in experiments that are performed out of laboratory conditions.

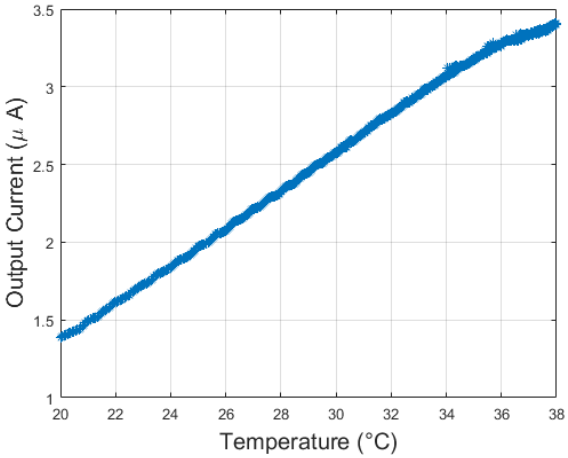

Fig. 8. Output current of the sensor related to the temperature of the solution in which it is immersed.

References

[1] R. M. Trujillo, D. E. Barraza, M. L. Zamora, A. Cattani-scholz, and R. E. Madrid, "Nanostructures in Hydrogen Peroxide Sensing," pp. 1–26, 2021.

[2] E. Sardini, M. Serpelloni, and S. Tonello, "Printed electrochemical biosensors: Opportunities and metrological challenges," *Biosensors*, vol. 10, no. 11, 2020, doi: 10.3390/bios10110166.

[3] S. Jo, D. Sung, S. Kim, and J. Koo, "A review of wearable biosensors for sweat analysis," *Biomed. Eng. Lett.*, vol. 11, no. 2, pp. 117–129, 2021, doi: 10.1007/s13534-021-00191-y.

[4] M. Majdinasab, M. Daneshi, and J. Louis Marty, "Recent developments in non-enzymatic (bio)sensors for detection of pesticide residues: Focusing on antibody, aptamer and molecularly imprinted polymer," *Talanta*, vol. 232, no. April, p. 122397, 2021, doi: 10.1016/j.talanta.2021.122397.

[5] H. Karimi-Maleh, F. Karimi, M. Alizadeh, and A. L. Sanati, "Electrochemical Sensors, a Bright Future in the Fabrication of Portable Kits in Analytical Systems," *Chem. Rec.*, vol. 20, no. 7, pp. 682–692, 2020, doi: 10.1002/tcr.201900092.

[6] K. Parate *et al.*, "Aerosol-jet-printed graphene electrochemical histamine sensors for food safety monitoring," *2D Mater.*, vol. 7, no. 3, 2020, doi: 10.1088/2053-1583/ab8919.

[7] E. Cantù, S. Tonello, G. Abate, D. Uberti, E. Sardini, and M. Serpelloni, "Aerosol jet printed 3D electrochemical sensors for protein detection," *Sensors (Switzerland)*, vol. 18, no. 11, pp. 1–14, 2018, doi: 10.3390/s18113719.

[8] Z. Lu *et al.*, "Novel flexible bifunctional amperometric biosensor based on laser engraved porous graphene array electrodes: Highly sensitive electrochemical determination of hydrogen peroxide and glucose," *J. Hazard. Mater.*, vol. 402, no. August 2020, p. 123774, 2021, doi: 10.1016/j.jhazmat.2020.123774.

[9] S. Tonello *et al.*, "Preliminary study of a flexible printed multi-sensing platform for electromyography and lactate measuring during rehabilitation," *2021 IEEE Int. Symp. Med. Meas. Appl. MeMeA 2021 - Conf. Proc.*, 2021, doi: 10.1109/MeMeA52024.2021.9478729.

[10] T. Fapanni, E. Sardini, M. Serpelloni, and S. Tonello, "3D Electrochemical Sensor and Microstructuration Using Aerosol Jet Printing," *Sensors*, vol. 21, no. 23, 2021, doi: 10.3390/s21237820.

[11] M. Borghetti, E. Cantù, E. Sardini, and M. Serpelloni, "Future sensors for smart objects by printing technologies in Industry 4.0 scenario," *Energies*, vol. 13, no. 22, 2020, doi: 10.3390/en13225916.

[12] N. G. Di Novo, E. Cantù, S. Tonello, E. Sardini, and M. Serpelloni, "Support-material-free microfluidics on an electrochemical sensors platform by aerosol jet printing," *Sensors (Switzerland)*, vol. 19, no. 8, 2019, doi: 10.3390/s19081842.

[13] X. Liu, Y. Zhou, J. Liu, and H. Xia, "The intrinsic enzyme mimetic activity of platinum oxide for biosensing of glucose," *Spectrochim. Acta - Part A Mol. Biomol. Spectrosc.*, vol. 248, no. 9, p. 119280, 2021, doi: 10.1016/j.saa.2020.119280.

[14] Y. Hu, M. Hojamberdiev, and D. Geng, "Recent advances in enzyme-free electrochemical hydrogen peroxide sensors based on carbon hybrid nanocomposites," *J. Mater. Chem. C*, vol. 9, no. 22, pp. 6970–6990, 2021, doi: 10.1039/d1tc01053k.

[15] G. Maduraiveeran and W. Jin, "Carbon nanomaterials: Synthesis, properties and applications in electrochemical sensors and energy conversion systems," *Mater. Sci. Eng. B Solid-State Mater. Adv. Technol.*, vol. 272, no. July, p. 115341, 2021, doi:

10.1016/j.mseb.2021.115341.

[16] S. S. Ghoreishizadeh, G. Nanda, S. Carrara, and G. De Micheli, “Empirical study of noise dependence in electrochemical sensors,” *Proc. 2013 5th IEEE Int. Work. Adv. Sensors Interfaces, IWASI 2013*, pp. 36–39, 2013, doi: 10.1109/IWASI.2013.6576080.

[17] H. Lee *et al.*, “A graphene-based electrochemical device with thermoresponsive microneedles for diabetes monitoring and therapy,” *Nat. Nanotechnol.*, vol. 11, no. 6, pp. 566–572, 2016, doi: 10.1038/nnano.2016.38.

[18] A. Hassibi, R. Navid, R. W. Dutton, and T. H. Lee, “Comprehensive study of noise processes in electrode electrolyte interfaces,” *J. Appl. Phys.*, vol. 96, no. 2, pp. 1074–1082, 2004, doi: 10.1063/1.1755429.

[19] S. T. Larsen, M. L. Heien, and R. Taboryski, “Amperometric noise at thin film band electrodes,” *Anal. Chem.*, vol. 84, no. 18, pp. 7744–7749, 2012, doi: 10.1021/ac301136x.

[20] L. Bahadori *et al.*, “The Effect of Temperature on Kinetics and Diffusion Coefficients of Metallocene Derivatives in Polyol-Based Deep Eutectic Solvents,” *PLoS One*, vol. 10, no. 12, 2015, doi: 10.1371/journal.pone.0144235.